The development of a space climatology: 1. solar-wind magnetosphere coupling as a function of timescale and the effect of data gaps

Article

Supplemental Material

Lockwood, M. ORCID: https://orcid.org/0000-0002-7397-2172, Bentley, S. N., Owens, M. J. ORCID: https://orcid.org/0000-0003-2061-2453, Barnard, L. A. ORCID: https://orcid.org/0000-0001-9876-4612, Scott, C. J. ORCID: https://orcid.org/0000-0001-6411-5649, Watt, C. E. and Allanson, O. (2019) The development of a space climatology: 1. solar-wind magnetosphere coupling as a function of timescale and the effect of data gaps. Space Weather, 17 (1). pp. 133-156. ISSN 1542-7390 doi: 10.1029/2018SW001856 Available at https://centaur.reading.ac.uk/78209/

Space Weather

Supporting Information for

The development of a space climatology: 1. Solar-wind magnetosphere coupling as a function of timescale and the effect of data gaps

Mike Lockwood[1], Sarah N. Bentley[1], Mathew J. Owens[1], Luke A. Barnard[1], Chris J. Scott[1], Clare E. Watt[1] and Oliver Allanson[1]

Paper accepted by Space Weather, July 2018. doi: 10.1029/2018SW001856

[1]Department of Meteorology, University of Reading, Earley Gate, P.O. Box 243, Reading, Berkshire, RG6 6BB, UK

Contents of this file

1. A study of the relationships between the am index and the auroral electrojet indices. (Figures S1 to S4).
2. Plots analyzing the effect of data gaps (with methods A-D to handle them) on the determination of optimum coupling exponent α from the analysis of power input to the magnetosphere, P_α and the *am* geomagnetic index (Figures S5-S8)
3. Plots equivalent to those in the main text, but for the *ap* geomagnetic index rather than the *am* index. (Figures S9-S16)

Introduction

Part 1

This supporting information demonstrates the relationship between mid-latitude range indices and auroral electrojet indices, as mentioned in the main text . The relationship is studied using scatter plots of coincident data for averaging timescales, τ, of: (Figure S1) three hours; (Figure S2) one day; (Figure S3) twenty-seven days; and (Figure S4) one year.

- The auroral indices used are the standard AE(12), AU(12) and AL(12) indices generated by the World Data Center for Geomagnetism, Kyoto
- AE data are available from http://wdc.kugi.kyoto-u.ac.jp/aedir/index.html
- The range index used is the same as in the main paper, namely the planetary *am* index generated by by L'École et Observatoire des Sciences de la Terre (EOST), a joint of the

University of Strasbourg and the French National Center for Scientific Research (CNRS) institute, on behalf of the International Service of Geomagnetic Indices (ISGI).

- *am* data are available from http://isgi.unistra.fr/data_download.php
- Plots are for data from 1968-2017, inclusive for when AU and AL data are available as well as AE (for 1957-1968 only AE data are available and the distribution of stations used was different). Hourly means of the AE indices were used and averaged over the same 3-hour intervals that *am* is derived over
- Unlike the *am* data, the AE data series are not completely continuous.
- All correlations are significant to greater than the 99.99% level using the AR-1 noise model to account or autocorrelation in the two data series.
- At higher activity levels (increased *am*, AE and AU and increasingly negative, AL) the AE(12) indices tend to saturate because the auroral oval expands equatorward of the ring of 12 stations used compile them.
- AL monitors the night sector (westward) auroral electrojet which is enhanced during substorm expansion/recovery phases.
- AU monitors the dayside eastward electrojet and is enhanced during all substorm phases
- AE responds to all substorm, being the sum of the two

Part 2

Plots in Parts 2 are in the same format as Figures 10 and 11 in the main text (see main paper for details)

- These plots analyse the effect on correlations between power input to the magnetosphere, P_α and the *am* geomagnetic index (as used in the main paper) of deploying different methods of handling data gaps.
- Plots for the methods (A-D) are presented. These are summarized in the main text.

Part 3

Part 3 uses correlations between power input to the magnetosphere, P_α and the *ap* geomagnetic index (instead of the *am* index used in main text)

- The behavior using these two different planetary geomagnetic indices is very similar but the optimum coupling exponents α_p are slightly but consistently higher for *ap* than for *am*.
- Whereas there is no detectable variation in the optimum α_p using *am*, there is a small one (but still not statistically significant) using *ap*. We attribute this to a ~20% variation in the *ap* response with time-of-day and time of year compared to a corresponding variation of < 2.5% for *am*. (see paper: Lockwood, M., A. Chambodut, I.D. Finch, L.A. Barnard, M.J. Owens (2018) Time-of-day / time-of-year response functions of planetary geomagnetic indices).

Part 1 The relationships between am and the auroral indices

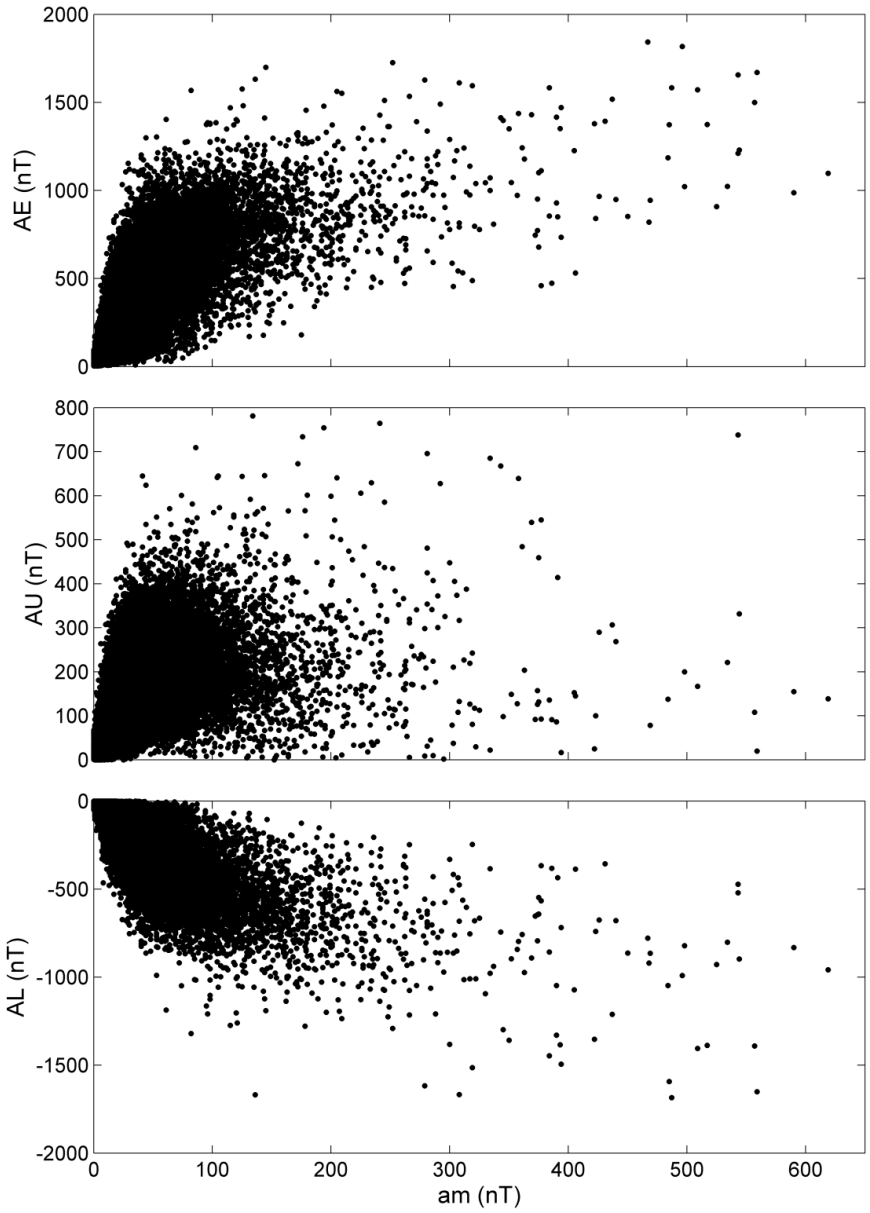

Figure S1. Scatter plot of 3-hourly values (top) the AE; (middle) the AU and (bottom) the AL index as a function of *am*. Even though the scatter in the data is large, the saturation of the AE indices with increasing activity, as quantified by the am index, is clearly seen. There are 136112 3-hourly data points and the linear correlation coefficient is $r = 0.788 \pm 0.002$ for AE and *am.*

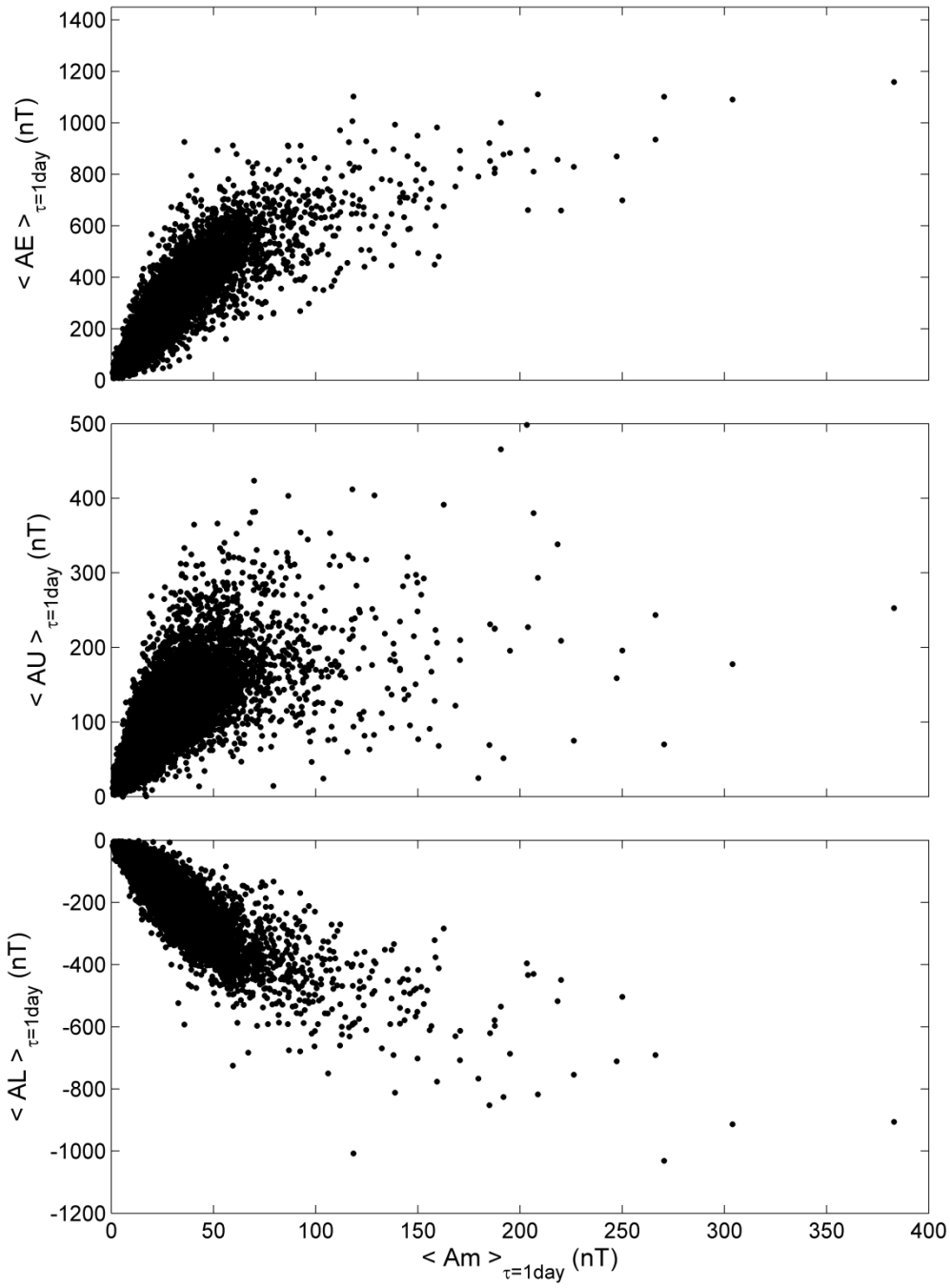

Figure S2. Scatter plot of one-day means of (top) the AE; (middle) the AU and (bottom) the AL index as a function of daily means of *am* (*Am*). The scatter is greater for AU mainly because of the strong seasonal variation in dayside polar ionospheric conductivities, whereas the conductivities in the nightside auroral electrojet influencing AL are more controlled by activity level because of the effects of particle precipitation . The scatter in AE is more than that in AL but less than that in AU. There are 17014 1-day-mean data points and the linear correlation coefficient is $r = 0.861 \pm 0.004$ for AE and *Am.*

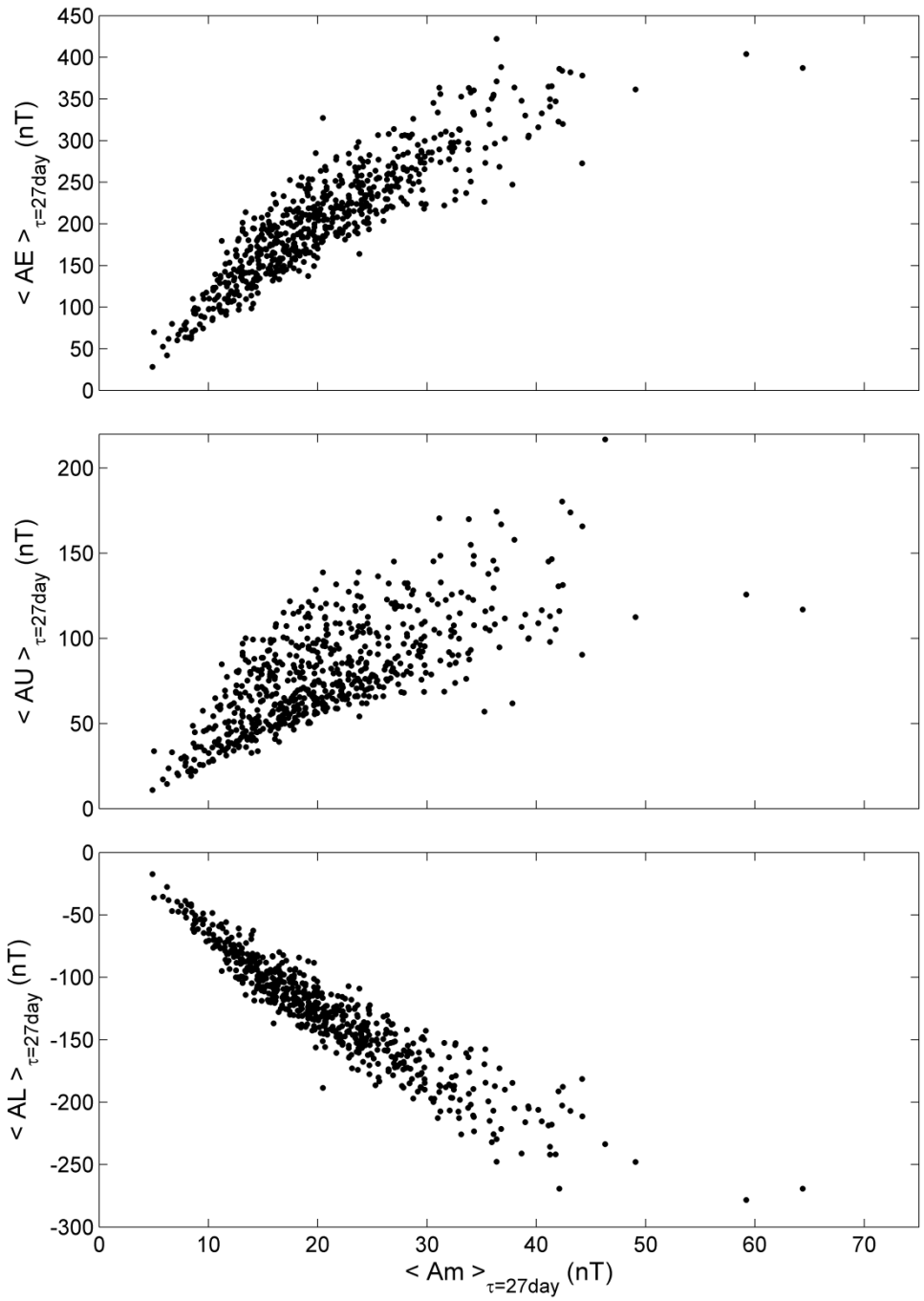

Figure S3. Scatter plot of 27-day (solar rotation period) means of (top) the AE; (middle) the AU and (bottom) the AL index as a function of *am*. The longer averaging period reduces the scatter but the seasonal conductivity effect remains. There are 627 27-day-mean data points and the linear correlation coefficient is $r = 0.89 \pm 0.02$ for AE and *am*.

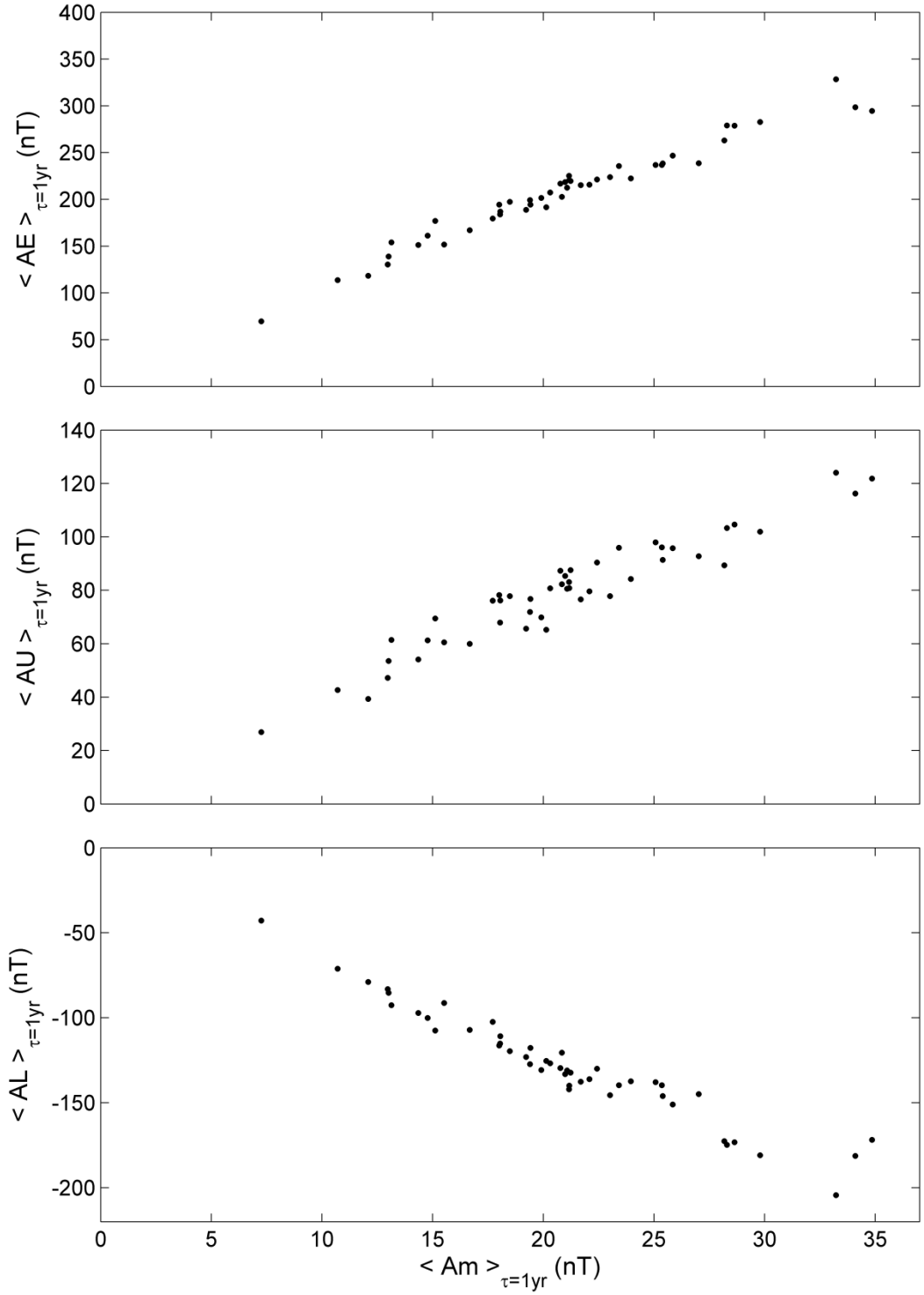

Figure S4. Scatter plot of 1-year means of (top) the AE; (middle) the AU and (bottom) the AL index as a function of Ap. The longer averaging period reduces the scatter and the seasonal conductivity effect remains. There are 47 annual-mean data points and the linear correlation coefficient is $r = 0.98 \pm 0.01$ for AE and *am*.

Part 2. Data gap analysis plots using the geomagnetic am index using all 4 methods to deal with data gaps

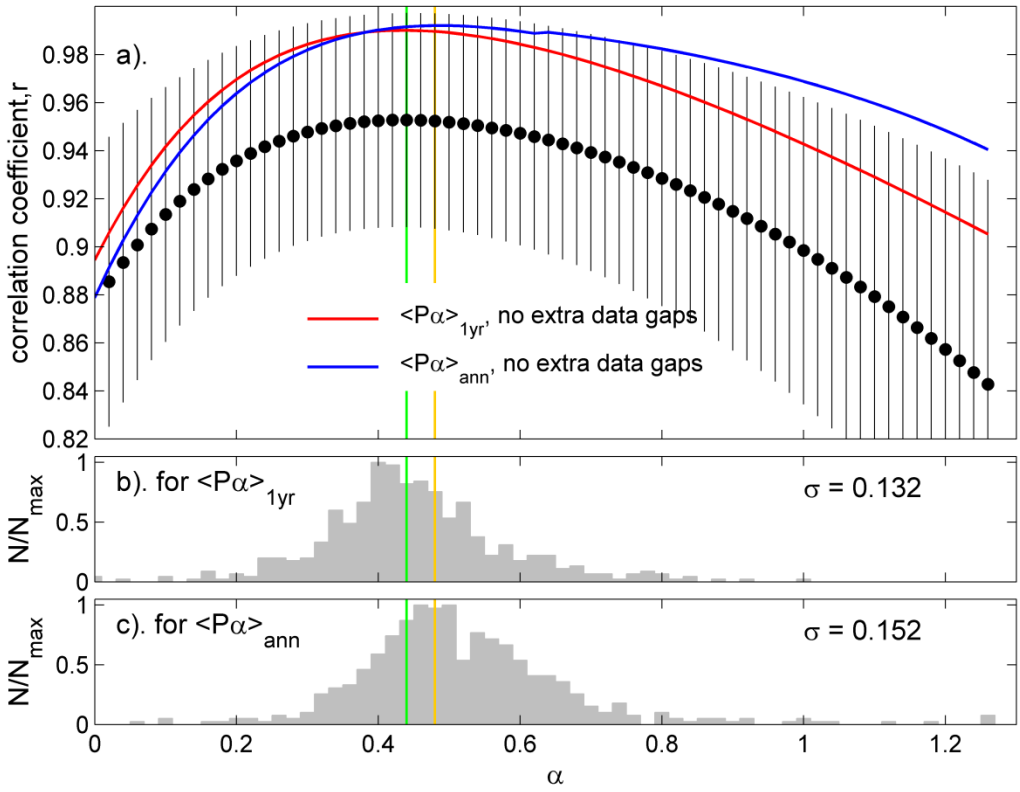

Figure S5. Analysis of the effect of data gaps using Method A (the algorithm of *Lockwood and Finch* [2007]) and the *am* index. This plot is in the same format and for the same conditions and analysis as Figure 10 of the main text, but is for is for Method A: see main text and the legend to Figure 10 for further details.

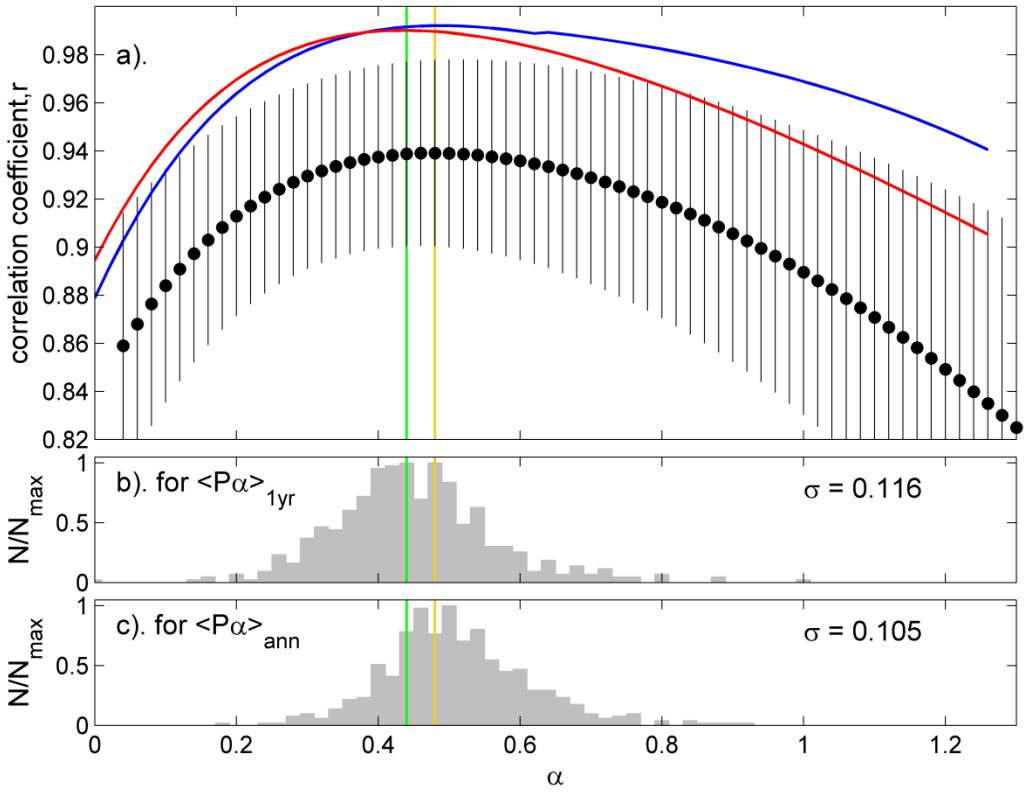

Figure S6. Analysis of the effect of data gaps using Method B (ignoring that they are present) and the *am* index. This plot is presented as Figure 10 in main text (included again here to aid comparisons).

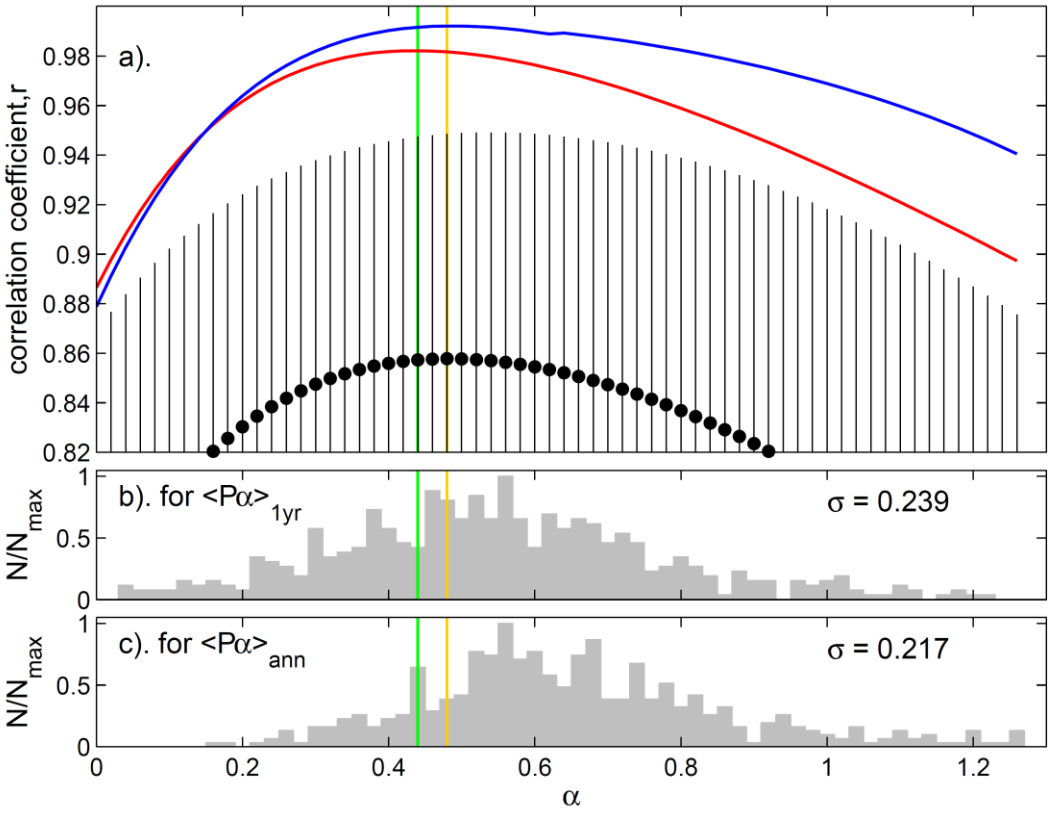

Figure S7. Analysis of the effect of data gaps using Method C (filling data gaps by linear interpolation) and the *am* index. This plot is in the same format and for the same conditions and analysis as Figure 10 of the main text, but is for is for Method C: see main text and the legend to Figure 10 for further details.

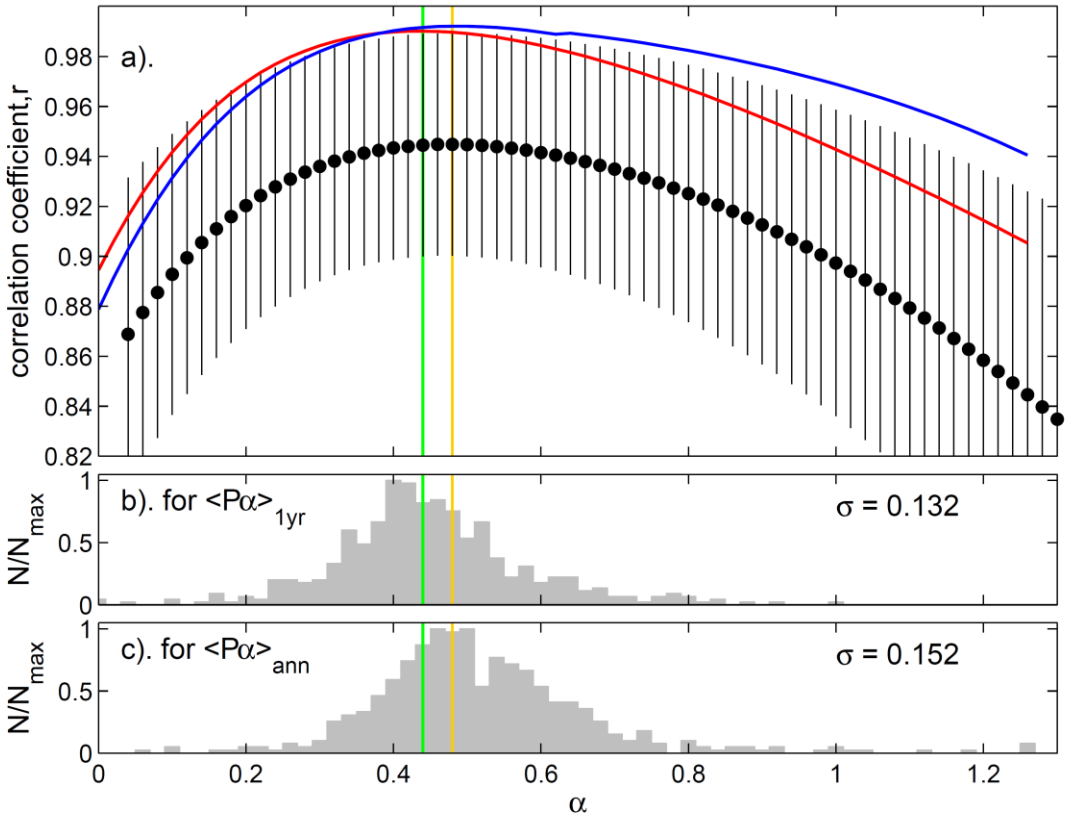

Figure S8. Analysis of the effect of data gaps using Method D (filling data gaps using Bartels rotation averaging and the interpolation procedure of *Svalgaard and Cliver* [2005]) and the *am* index. This plot is in the same format and for the same conditions and analysis as Figure 10 of the main text, but is for is for Method D: see main text and the legend to Figure 10 for further details.

Part 3. Results using the *ap* geomagnetic index

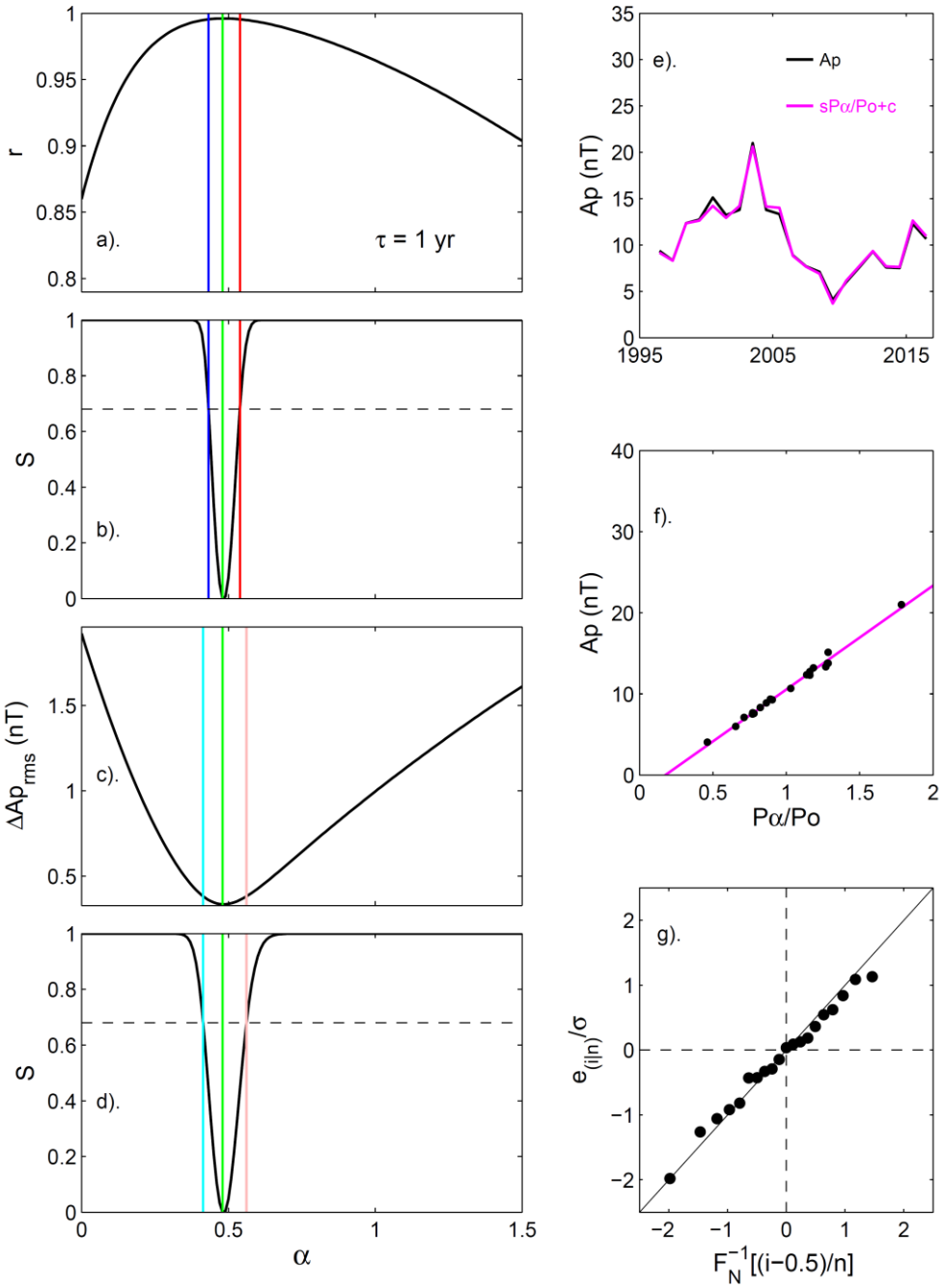

Figure S9. Analysis of correlation between power input to the magnetosphere, P_α, and the *ap* geomagnetic index for averaging timescale τ = 1 yr over the interval 1996-2016 (inclusive). This plot corresponds to Figure 4 of the main text, but is for the *ap* index rather than the *am* index.

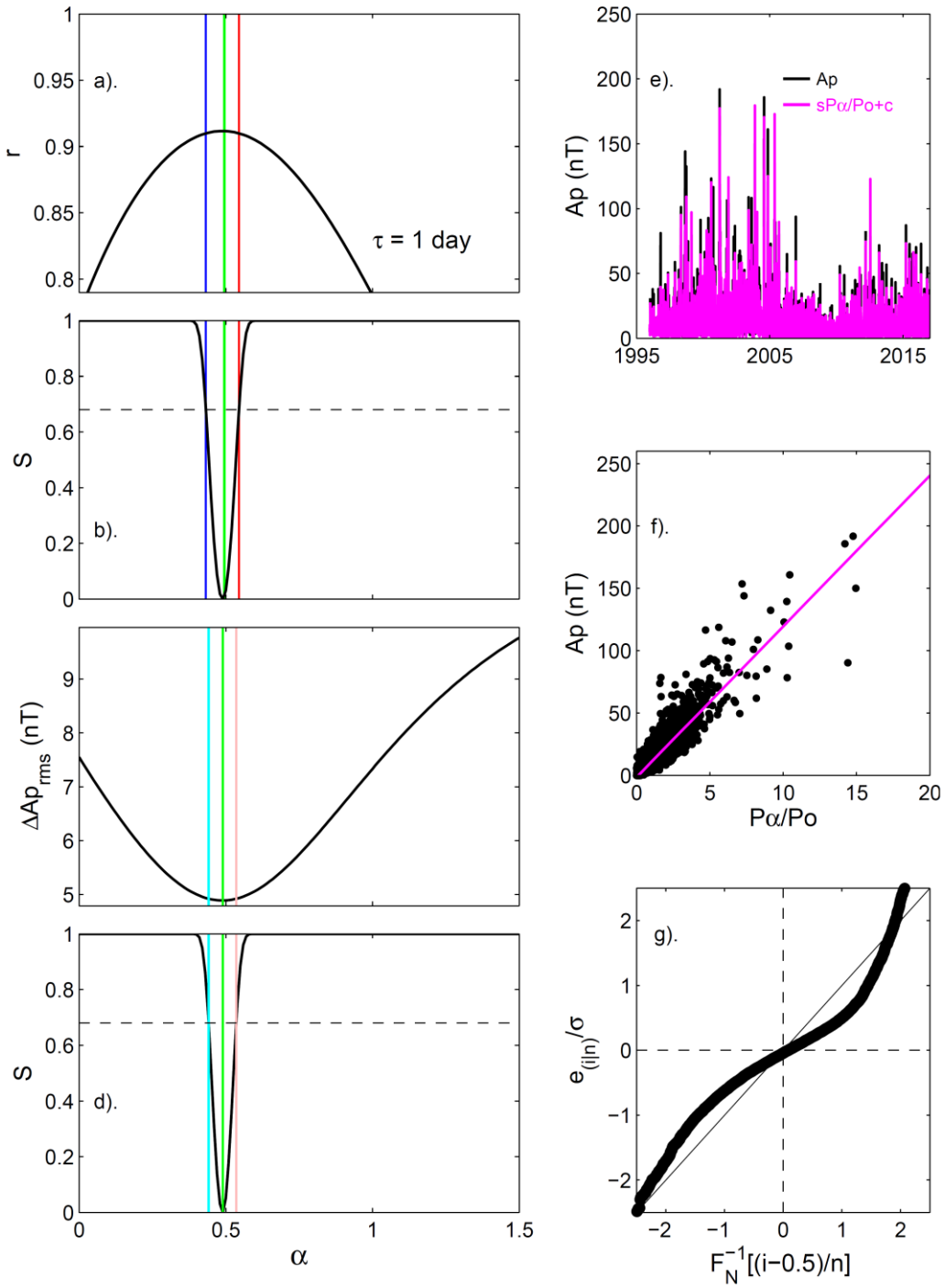

Figure S10. Analysis of correlation between power input to the magnetosphere, P_α, and the *ap* geomagnetic index for averaging timescale τ = 1 day over the interval 1996-2016 (inclusive). This plot corresponds to Figure 5 of the main text, but is for the *ap* index rather than the *am* index. Comparison of part (g) with Figure 5g shows that at this τ, departures from a normal distribution are more severe for *ap* than *am*.

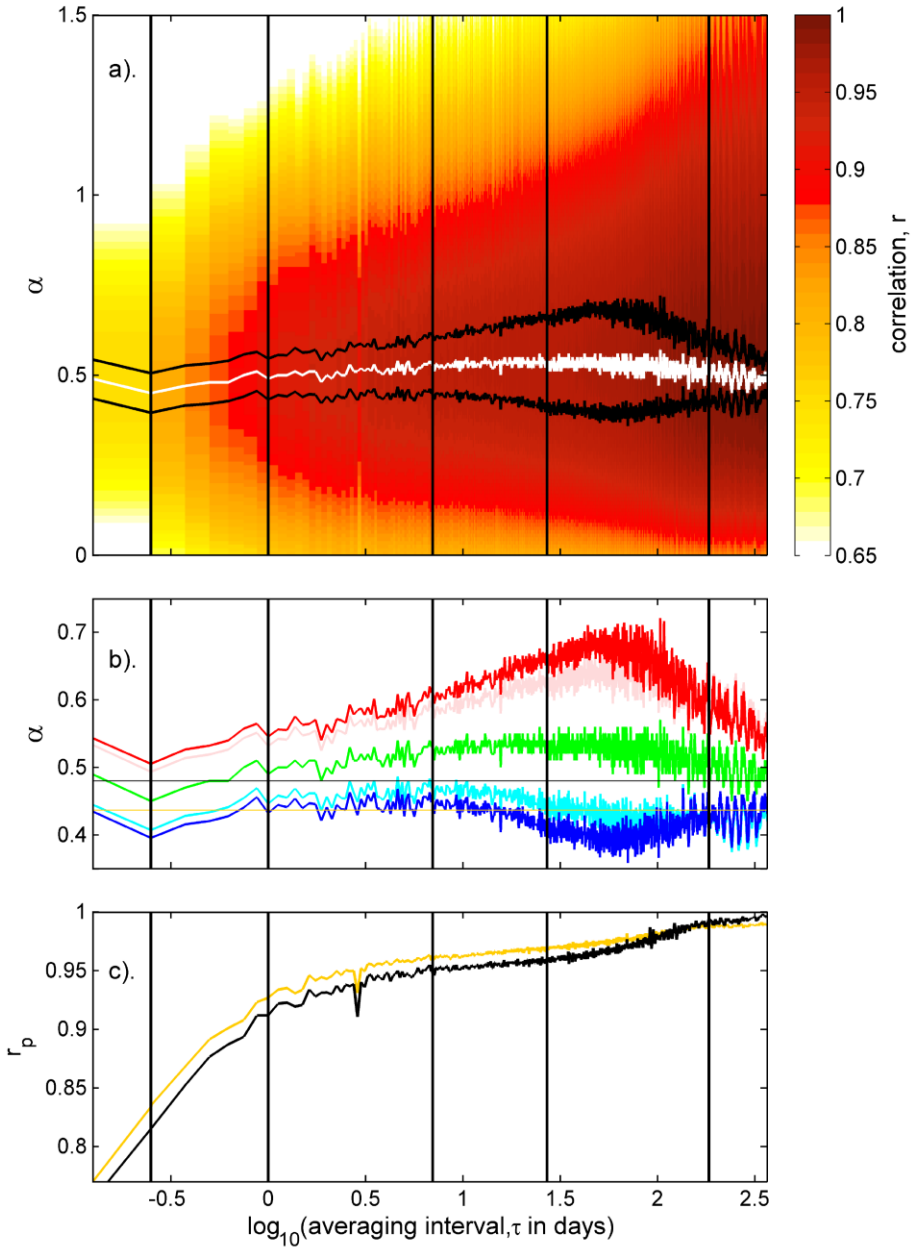

Figure S11. Correlation between $\langle ap \rangle_\tau$ and $\langle P_\alpha \rangle_\tau$ for the interval 1996-2016 (inclusive). This plot corresponds to Figure 6 of the main text, but is for the *ap* index rather than the *am* index. Note that the scale in (b) is different to that used in Figure 6 because α_p values are a bit higher for *ap* than for *am*. The orange horizontal line in (b) is the average α_p for the *am* index and the black line is α_p for *ap* at τ = 1yr. It can be seen that for *ap*, α_p is similar for $\tau \leq 1$ day and τ = 1yr, but consistently larger at τ in between. Values of α_p are consistently higher for *ap* than for *am*, but not by more than the estimated uncertainties. In (c) the orange curve is for *am* (as given in Figure 6c) and the black line for *ap*. For τ > 0.5 yr, $\langle ap \rangle_\tau$ and $\langle P_\alpha \rangle_\tau$ correlate slightly better than $\langle am \rangle_\tau$ and $\langle P_\alpha \rangle_\tau$ but the converse is true at τ < 0.5 yr. We attribute this to an exaggerated (by of order 20%) semi-annual variation in *ap*.

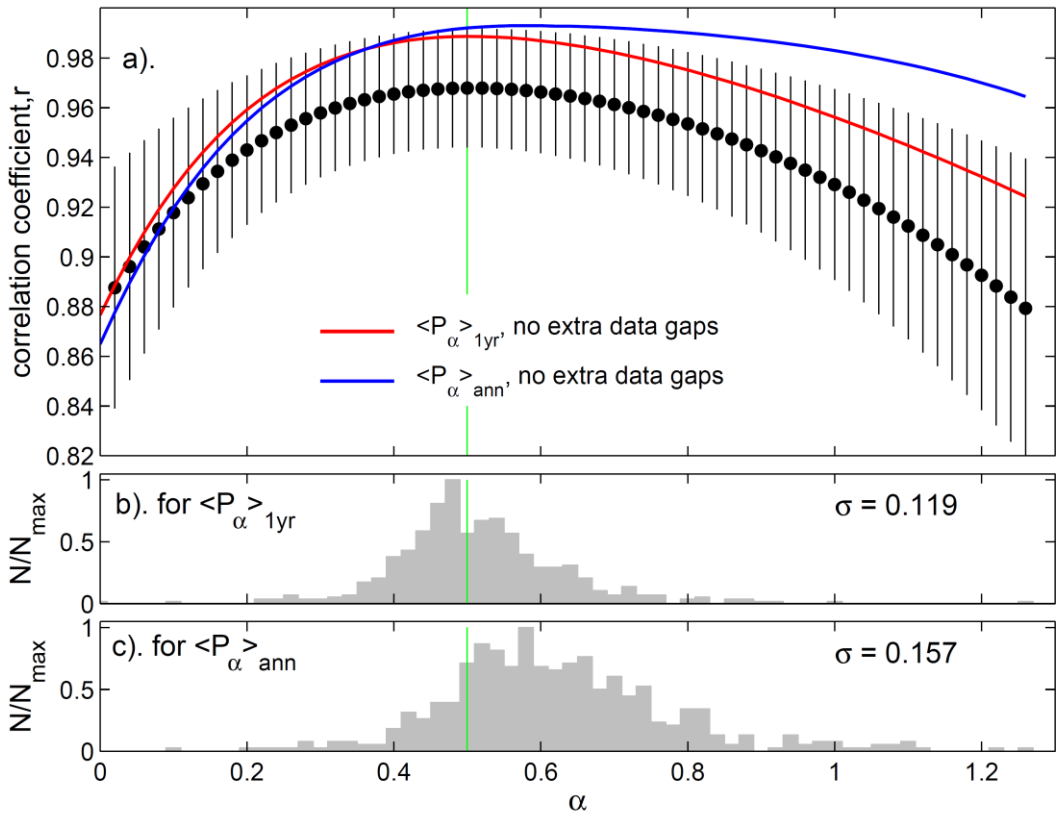

Figure S12. Analysis of the effect of data gaps using Method A (the algorithm of *Lockwood and Finch* [2007]). This plot corresponds to Figure S5, but is for is for the *ap* index rather than the *am* index.

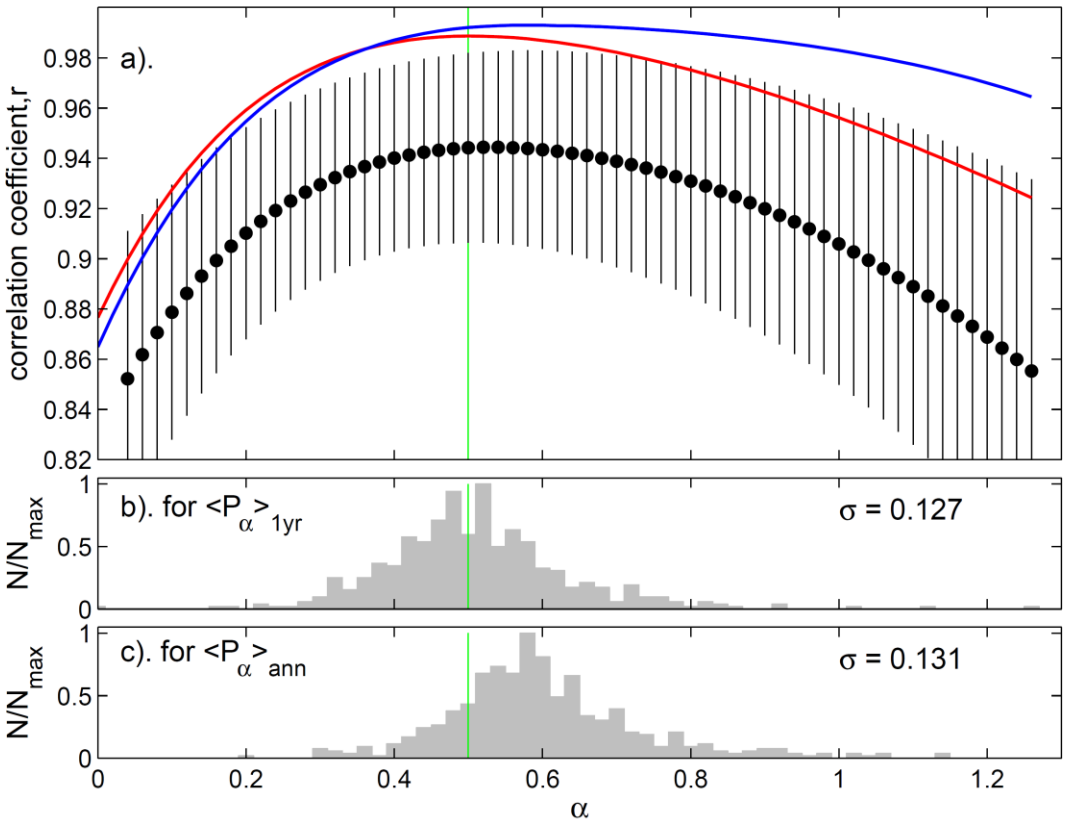

Figure S13. Analysis of the effect of data gaps using Method B (neglecting data gaps). This plot corresponds to Figure S6, but is for is for the *ap* index rather than the *am* index.

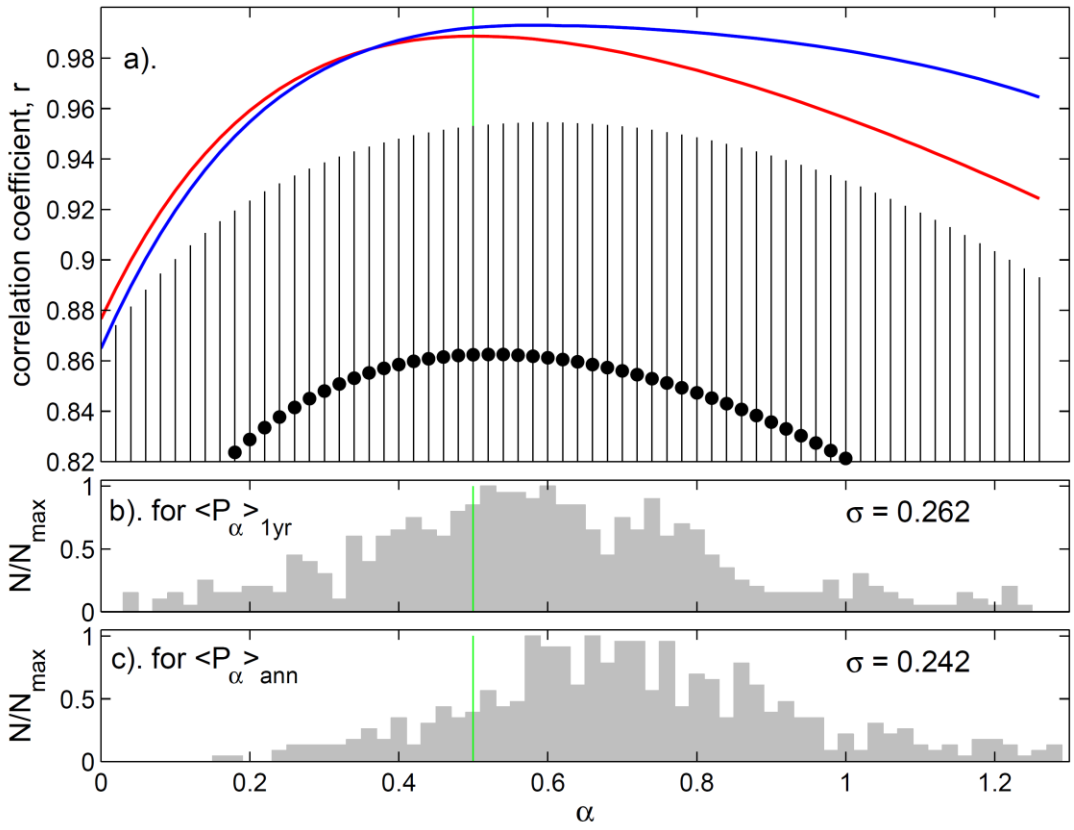

Figure S14. Analysis of the effect of data gaps using Method C (filling data gaps using linear interpolation). This plot corresponds to Figure S7, but is for is for the *ap* index rather than the *am* index.

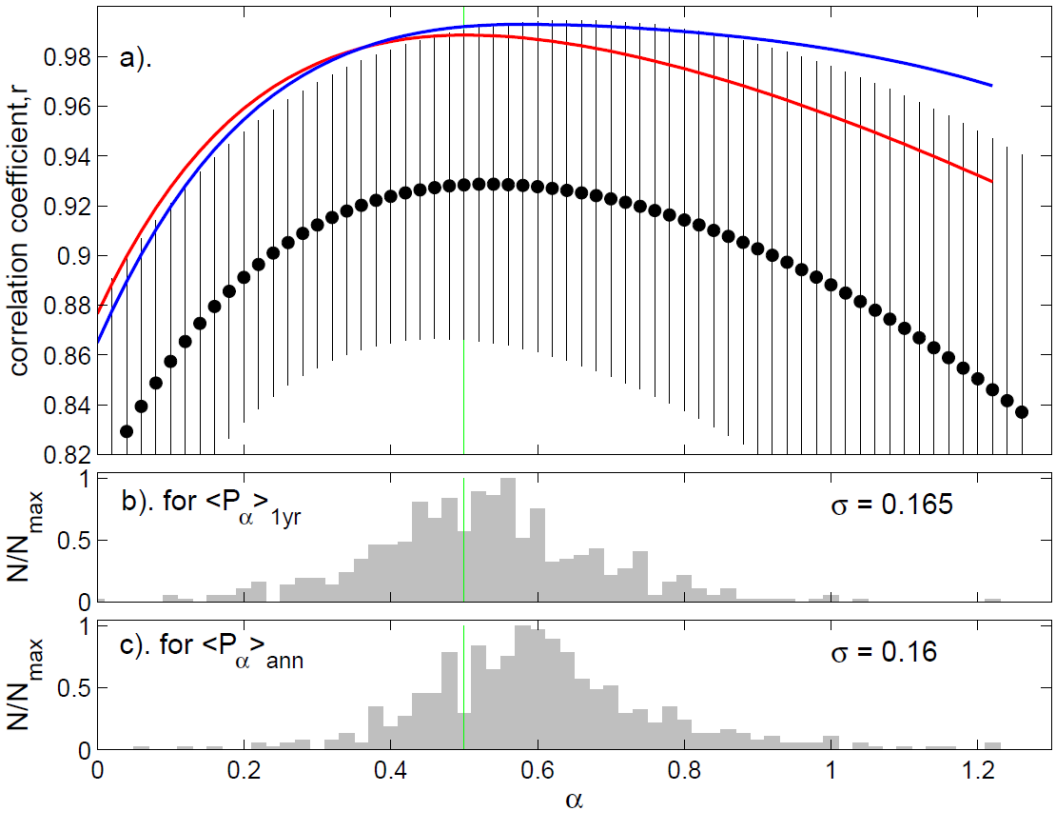

Figure S15. Analysis of the effect of data gaps using Method D (using Bartels rotation averaging and the interpolation procedure of *Svalgaard and Cliver* [2005]). This plot corresponds to Figure S8, but is for is for the *ap* index rather than the *am* index.

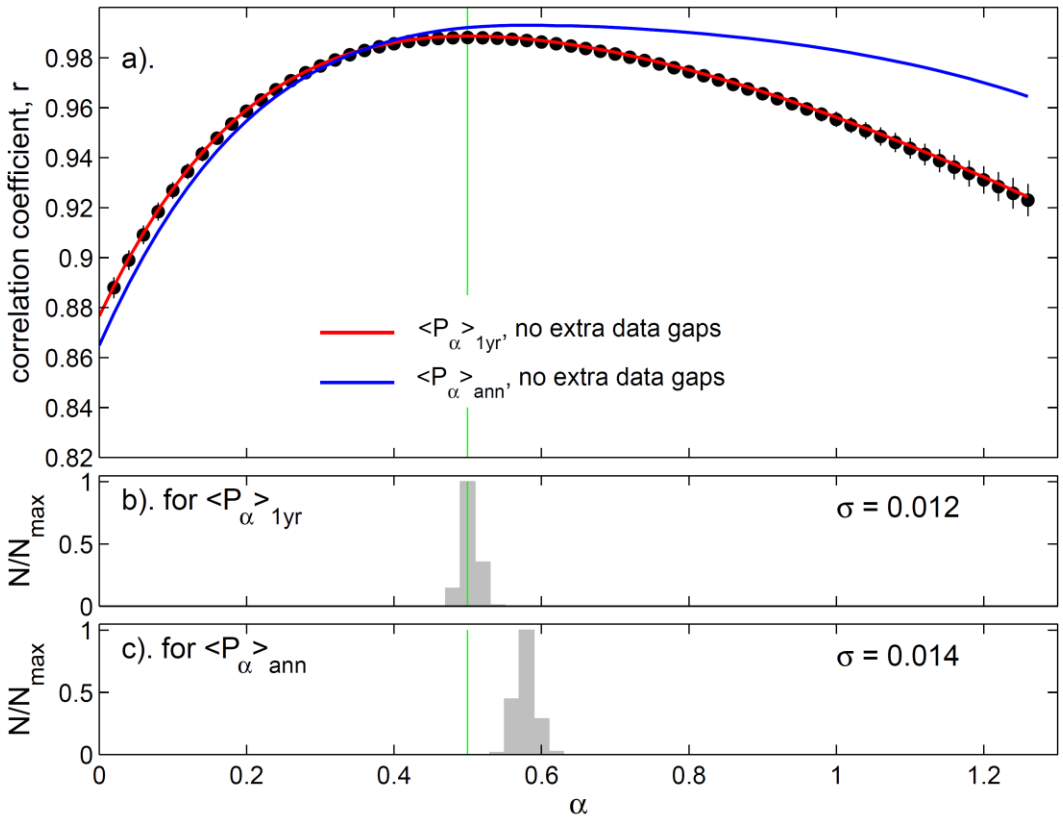

Figure S16. Analysis of the effect of data gaps using Method A (the algorithm of *Lockwood and Finch* [2007]) with data gap masks drawn from after 1995. This plot corresponds to Figure 11 of min text, but is for is for the *ap* index rather than the *am* index.